A New Facilitated Process of Biomass-Derived Furans to p-Xylene with Ethanol over Zeolite

Ivo F. Teixeira, Benedict T.W. Lo, Pavlo Kostetskyy, Michail Stamatakis, Lin Ye, Chiu C. Tang, Giannis Mpourmpakis and Shik Chi Edman Tsang

Reaction conditions:

In a typical experiment, 15 mL of the model compound 2,5-Dimethylfuran (99% Sigma-Aldrich), 8.2 mL of ethanol (99.5% Sigma-Aldrich) and 0.4 g of zeolite were used over a temperature range of 200 to 300 °C and 1.0 mL of tridecane as an internal standard. The reaction vessel was flushed with inert gas (N2). Liquid products were identified and quantified using a gas chromatograph/mass spectrometer (Agilent 6890 and Agilent MSD 5973 (N)) calibrated with pure standards. After reaction, the autoclave was cooled down to −60°C by dry ice/acetone bath. The gas products (CO, CO_2, CH_4) analyzed by a Perkin Elmer Autosystem XL Arnel Gas phase GC-FID-Methanator. C_2H_4 gas product was assumed to be mainly produced from ethanol. The solid residue was filtrated and washed with acetone and dried overnight (80 °C). Then it was analyzed by thermogravimetric analyses (TA instruments Q50), the samples were heated at 10 °C min^{-1} from room temperature to 900 °C under air to quantify the coke on zeolite to complete the carbon balance. The conversion was expressed in term of the molar conversion of 2,5-dimethylfuran and carbon balance was achieved at the minimum of 90-95%.

Assessment of a possible diffusional controlled (mass limitations) reaction:

The reaction conditions for ethylene gas or ethanol liquid placed with DMF liquid (generated pressurized vapors at 300^{o}C) were employed following the conditions established in reference [1], which carefully eliminated the potential for interphase mass transfer limitations. Weisz-Prater criterion was also considered based on our experimental parameters below. In any case, assuming ideal gases, the value of the Weisz-Prater coefficient is on the order of 10^{-14} to 10^{-15}, which indicates no mass transfer limitations[2,3]. In the liquid phase, the diffusion coefficients are typically up to 4 orders of magnitude smaller, and in that case the Weisz-Prater coefficient would be around 10^{-10}, indicating again no mass transfer limitations measuring the intrinsic kinetics. Thus, according to the calculations, there was no evidence on mass transfer limitation (the Weisz-Prater number is << 1 for all temperatures reported). For the calculation of the worst case scenario, i.e. the highest temperature and thus highest reaction rate was used.

The reaction between ethylene or ethanol with DMF (generated from pressurized vapors at 300°C) was studied, following the experimental protocol established in reference [1], carefully eliminating the possibility of mass transfer limitations. Assuming that under the reaction conditions all species behave as ideal gases, molecular diffusivities were calculated from the following equation (1):

$$D_{AB} = \frac{2}{3} \cdot \sqrt{\frac{k_B^{\,3}}{\pi^2}} \cdot \sqrt{\frac{1}{2 \cdot m_A} + \frac{1}{2 \cdot m_B}} \cdot \frac{4 \cdot T^{\frac{3}{2}}}{P \cdot \left(d_A + d_B\right)^2} \qquad (1)$$

where D_{AB} denotes the binary diffusion coefficient between ideal gases A and B, k_B Boltzmann's constant, m_A and m_B the mass of molecules A and B, respectively, T the temperature, P the pressure, and d_A and d_B the diameter of molecules A and B, respectively (estimated to 4.4 Å, 4.0 Å and 8.0 Å, respectively for ethanol, ethylene and DMF). Under experimental conditions that result in the lowest diffusivities (573 K, 140 bar) we obtain the following values for self- and binary diffusion:

D_{AB} (cm^2/s) B→ A↓	EtOH	Ethylene	DMF
EtOH	$1.992 \cdot 10^{-3}$	$2.513 \cdot 10^{-3}$	$8.629 \cdot 10^{-4}$
Ethylene		$3.089 \cdot 10^{-3}$	$1.103 \cdot 10^{-3}$
DMF			$4.172 \cdot 10^{-4}$

Moreover, Knudsen diffusivities were estimated from equation (2):

$$D_{Knudsen} = \frac{d_{pore}}{3} \cdot \sqrt{\frac{8 \cdot k_B \cdot T}{\pi \cdot m_A}} \qquad (2)$$

where $D_{Knudsen}$ denotes the Knudsen diffusion coefficient and d_{pore} the diameter of the pore of the zeolite. Under experimental conditions that result in the lowest diffusivities, and for the smallest pore diameter of 20 Å, we obtain the following values for the Knudsen diffusion coefficients:

$D_{Knudsen}$ (cm^2/s)	EtOH
EtOH	$3.421 \cdot 10^{-3}$
Ethylene	$4.384 \cdot 10^{-3}$
DMF	$2.369 \cdot 10^{-3}$

The effective diffusion coefficient was calculated for the slowest diffusing species DMF as follows:

$$D_{eff,DMF} = \left(\frac{1}{D_{DMF,DMF}} + \frac{1}{D_{Knudsen,DMF}} \right)^{-1} = 3.547 \cdot 10^{-4} \frac{cm^2}{s} \quad (3)$$

To assess the presence of mass transfer limitations the Weisz-Prater criterion was considered. The Weisz-Prater parameter was calculated as:

$$C_{WP} = \frac{R_{obs} \cdot \rho_c}{D_{eff} \cdot C_{reac}} \cdot \left(\frac{d_{particle}}{2} \right)^2 \quad (4)$$

where R_{obs} denotes the observed reaction rate, ρ_c the density of the catalytic particle, C_{reac} the concentration of the reactant, and $d_{particle}$ the particle diameter. Values of $C_{WP} << 1$ indicate that there are no mass transfer limitations. Under the conditions of the experiment (assuming ideal gas phases) we get a value of C_{WP} on the order of 10^{-14}. If there is condensation under the reaction conditions, the liquid phase diffusion coefficients would typically be expected to be up to 4 orders of magnitude lower and the densities up to 3 orders of magnitude higher. In this case, the Weisz-Prater coefficient would be around 10^{-13}, indicating again that there are no mass transfer limitations and that the intrinsic kinetics are indeed measured.[2,3]

Computational Methods

Ab-initio electronic structure calculations were performed to study the Brønsted acid-catalyzed (BA) p-xylene formation from ethanol and 2,5-dimethylfuran (DMF). Detailed reaction energetics were calculated at the M06-2X/6-311+G(d,p)[4] level of theory, as implemented in the Gaussian 09[5] package. The BA site of has been modeled as a proton in our calculations. The identical computational approach has been shown to be effective in calculating the reaction energetics in the production of p-xylene via cycloaddition between ethylene and DMF[6]. Reaction pathways were first mapped by scanning the potential energy surface (PES) along the reaction coordinate. The energy maximum found along each reaction coordinate was relaxed to a saddle point to locate the actual transition state. All transition states and local minima were obtained by full optimizations and verified by vibrational frequency and Intrinsic Reaction Coordinate (IRC) calculations[7]. In addition, proton affinities (PA) of all relevant reaction species were calculated at the CBS-QB3[8] level of theory, chosen for its accuracy in calculating gas-phase thermochemistries, as reported in our previous work[9]. PA was used to quantify the thermodynamic preference of the different species to bind the acidic proton and it is calculated according to Equation (1):

$$PA = E_{molecule+H^+} - E_{molecule} \quad (5)$$

where $E_{molecule+H}$ and $E_{molecule}$ are the total electronic energies of the protonated and neutral species, respectively, as the electronic energy of a proton is zero.

Table S1: Gas-phase proton affinities of reaction species calculated at the CBS-QB3 level of theory (negative values indicate exothermicity)

Species	PA (kJ/mol)
Ethanol	-779.1
p-Xylene	-770.8
DMF (O)	-732.3
Water	-682.2
Ethylene	-677.3

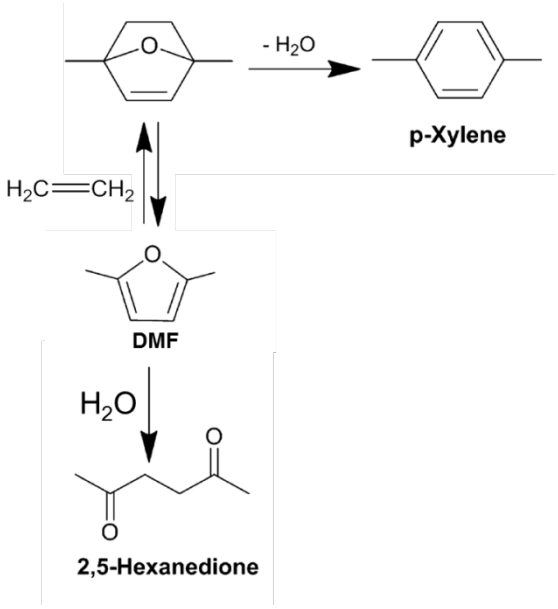

Figure S1. One-pot reaction to obtain p-Xylene from DMF and the main side reaction with water producing 2,5-Hexanedione (diketone).

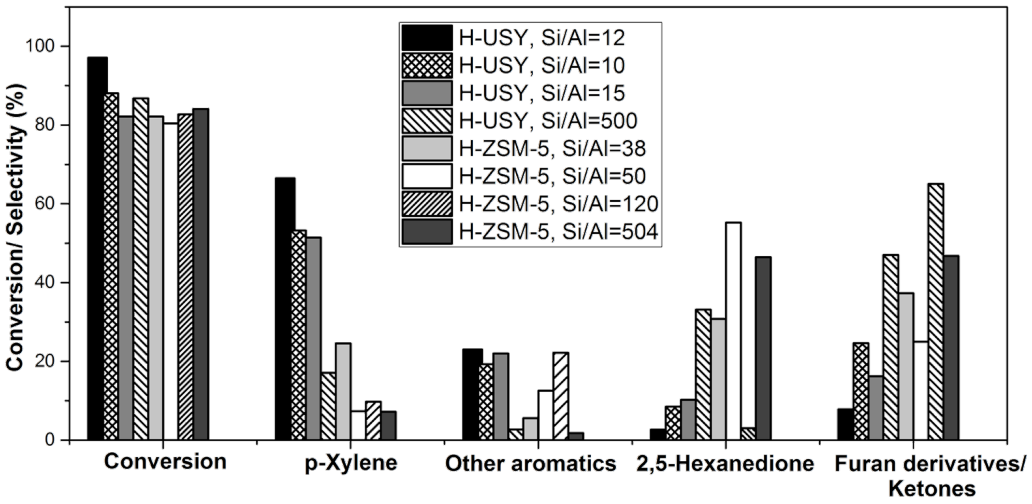

Figure S2. Conversion and selectivity for DMF transformation into aromatics catalyzed by different zeolites. Reaction conditions: temperature 300 °C, molar ratio ethanol/DMF 1:1 and reaction time 12 h.

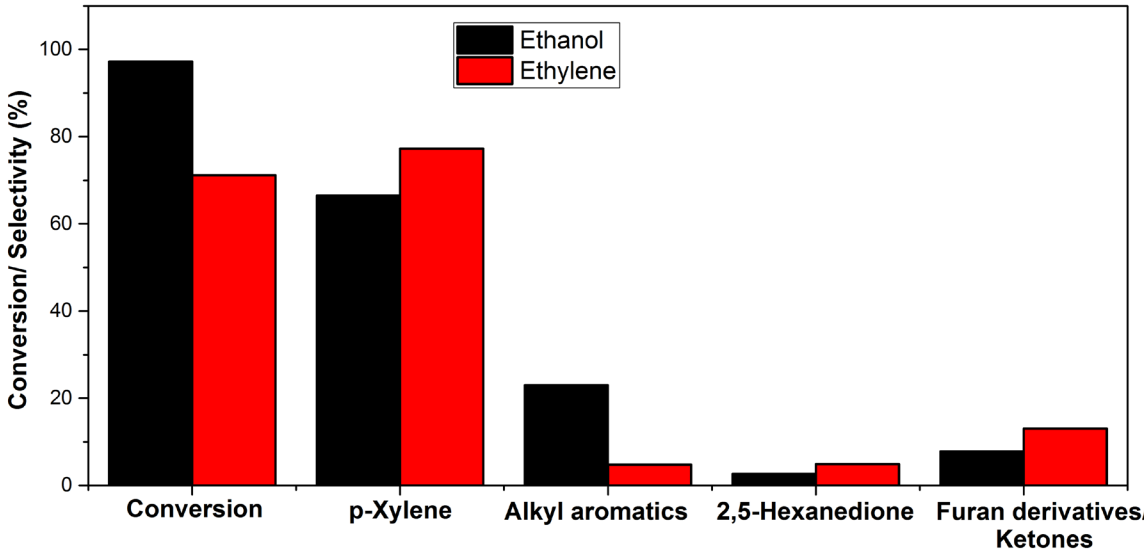

Figure S3. Conversion and selectivity for DMF transformation into aromatics catalyzed by zeolite HUSY (Si/Al=12) with ethylene generated in situ from ethanol compared with only pressure of ethylene (40 bar). The results showed about 95% conversion of 2,5 dimethyl-furan and 90% selectivity to aromatics (for example, 67% p-xylene, 23% 1-ethyl-2,5-dimethylbenzene, giving 85.5% carbon yield with respect to DMF). According to stoichiometry ethanol conversion was estimated to be completely converted to the aromatic products within experimental error. Reaction conditions: temperature 300 °C, molar ratio ethanol/DMF 1:1 and reaction time 12 h in 100mL reactor.

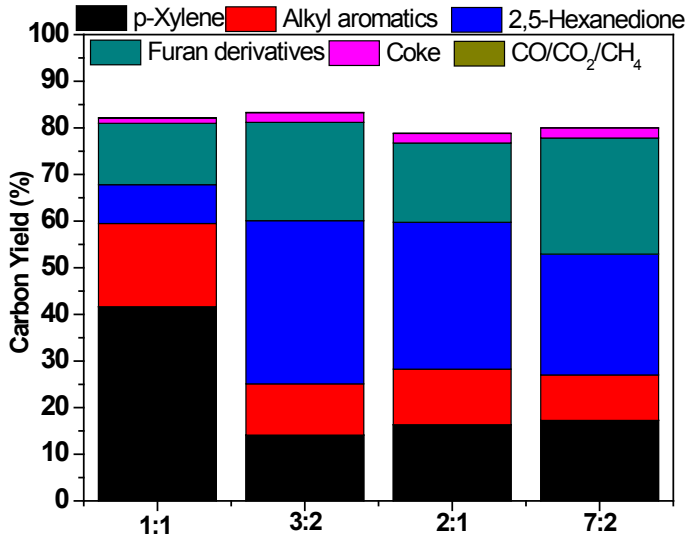

Figure S4. Conversion and carbon yield for DMF transformation into aromatics catalyzed by zeolite HUSY (Si/Al=15) with different molar ratios Ethanol/DMF. Reaction conditions: temperature 300 °C, molar ratio ethanol/DMF 1:1 and reaction time 12 h in 100mL reactor.

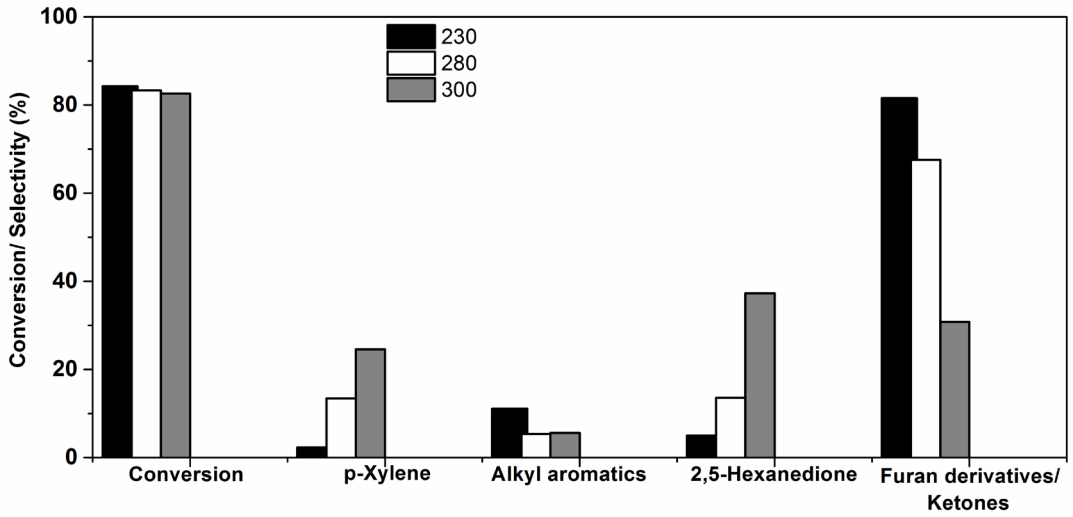

Figure S5. Conversion and selectivity for DMF transformation into aromatics catalyzed by zeolite HZSM-5 (Si/Al=38) at different temperatures. Reaction conditions: molar ratio ethanol/DMF 1:1 and reaction time 12 h in 100mL reactor.

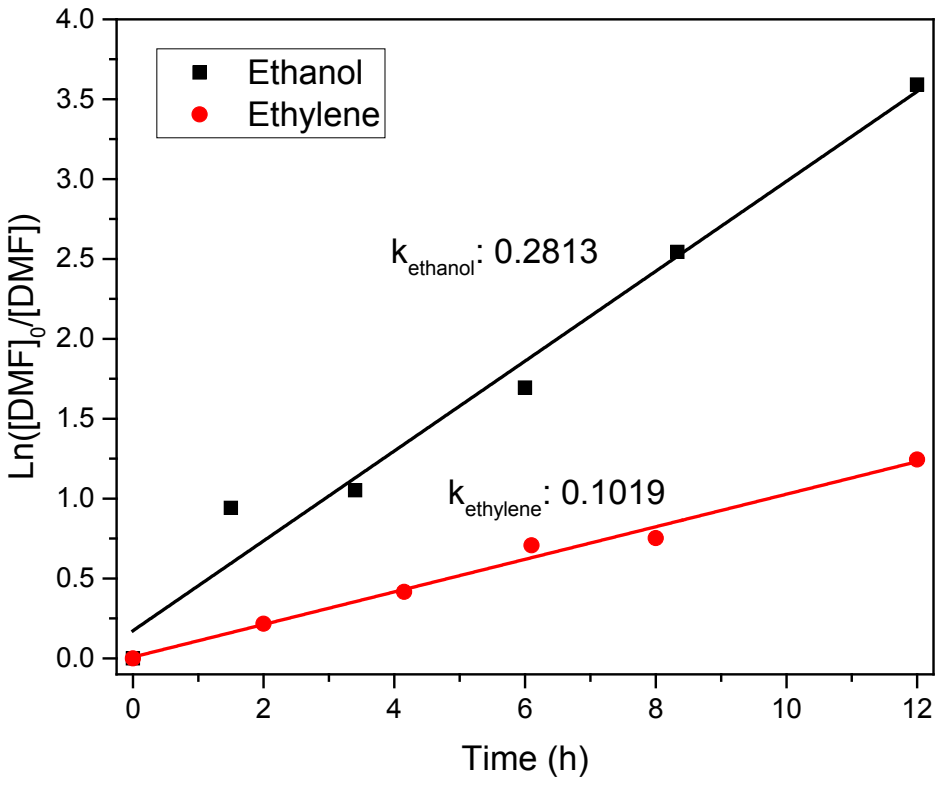

Figure S6. First order fitting and constant rate values for DMF transformation into aromatics catalyzed by zeolite HUSY (Si/Al=12) with ethylene generated in situ from ethanol and only pressure of ethylene (40 bar). Reaction conditions: temperature 300 °C in 100mL reactor.

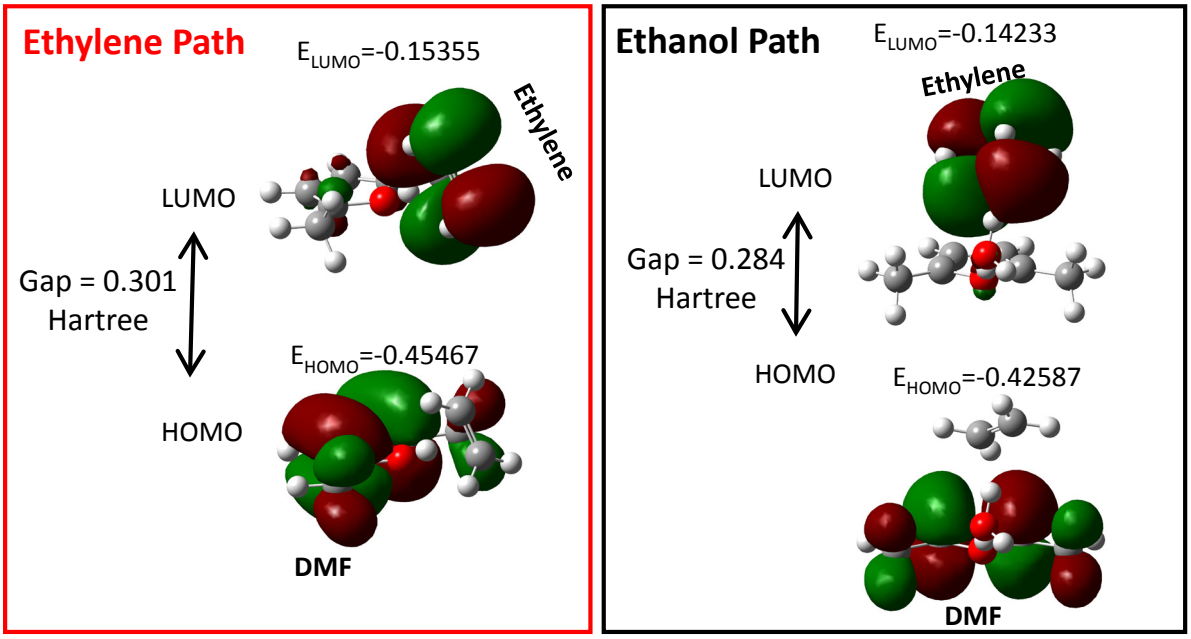

Figure S7. HOMO-LUMO orbital analysis and associated energy gaps in the initial state of the Diels-Alder (DA), [4+2] cycloaddition reaction. In the ethanol path, the ethylene molecule (dienophile) is stabilized through hydrogen bonds on top of the DMF (diene), orienting its LUMO orbital projection closer to the HOMO of the DMF as compared to that of DMF with a direct protonation in the case of ethylene path. In addition, the HOMO-LUMO energy gap in the ethanol path is substantially lower compared to that of the ethylene path. It is attributed to this spatial orientation of the HOMO-LUMO orbital overlap and the difference in charge density of H_3O^+ stabilized DMF from that of the direct protonated DMF, which results to the decrease in the overall DA barrier in the ethanol path.

Table S2. Reaction rate and reaction rate per mol of reactant (ethanol or ethyele) for DMF transformation into aromatics per gram of zeolite HUSY (Si/Al=12) with ethylene generated in situ from ethanol and only pressure of ethylene (40 bar). Reaction conditions: temperature 300 °C.

Substrate	Rate (mol/g.h)	Rate ($mol_{DMF}/mol_{EtOH/C2H4}$.g.h)
Ethanol	0.141	1.017
Ethylene	0.034	0.075

Synchrotron X-ray powder diffraction (SXRD) and Rietveld refinements

SXRD data were collected on Beamline I11, Diamond Light Source, Harwell, UK.[10] The energy of the incident X-ray flux was set at 15 keV. The wavelength and the 2θ-zero point were refined using a diffraction pattern obtained from a high quality silicon powder (SRM640c), corresponding to (i) for pyridine data: λ = 0.825634(2) Å and $2\theta_{ZP}$ = -0.002500(10)° and (ii) for ammonia data: λ = 0.826617(4) Å and $2\theta_{ZP}$ = -0.000254(10)°. High resolution SXRD data were obtained from the zeolite samples using the multi-analyser crystals (MAC) detectors. The patterns were collected in the 2θ range 0-150° with 0.001° data binning. Each MAC pattern was collected for an hour for good statistics. In total, there are 4190 *hkl* reflections measured over the range of 3-55°, of which at least 300 independent *hkl* reflections are observed. From a crystallography perspective, the number of structural variables should not exceed the number of *hkl* reflections in a refinement. In the Rietveld refinements performed in this work, the number of structural parameters has not exceeded 170.

Using the TOPAS software, the lattice parameters were refined using Le Bail method, and also the Rietveld refinement analyses of the diffraction patterns were performed. The starting coordinates used were based on the H-ZSM-5 zeolite model by Heo *et al.* for sample refinement.[11] The background curve was fitted by a Chebyshev polynomial with an average of 20 coefficients. The Thompson-Cox-Hastings pseudo-Voigt peak function proposed by Thompson *et al.* was applied.[12] The scale factor and lattice parameters were allowed to vary for all the histograms. The refined structural parameters for each data histogram were the fractional coordinates (*x,y,z*) and isotropic displacement factors (B_{eq}) for all atoms, and the site occupancy factors (SOF), translation and rotation axes for the two rigid body Z-matrices describing the adsorbate molecules within the zeolitic framework (with fixed bond distance and angles). The B_{eq} were constrained in the following way: all the T-sites (T=Al, Si) share the same value, and the values for the O-sites are twice the B_{eq} for the T-sites. A restraint was applied to the distance on the hydrogen atoms between the adsorbate molecules (an anti-bump command in TOPAS) [H^*-H_a^* > 2.2], and the weighting was slowing reduced to 10 at the final stage of the refinement. The crystallographic data at 25 °C and refinement details are summarised in Tables S3 – S6. The position errors of the atoms of the adsorbate molecules are estimated from the percentage errors of the translation axis.

The zeolite sample was firstly treated under vacuum at 200 °C for 2 hours before it was adsorbed with ethanol and/or DMF vapor from their liquid(s). For pure ethanol or DMF uptake experiment, saturated vapor pressure of adsorbate was used. For the equimolar ethanol-DMF uptake experiment, an equimolar mixture of ethanol-DMF from liquids was used to provide the mixed vapors. The total molar amount of liquid introduced to the reactor chamber containing the zeolite was set at 75% of the total mole of Brønsted acid sites as in our previous NMR and ICP experiments.

Crystallographic and atomic parameters

From Rietveld refinements of the SXRD data, the crystallographic details of the zeolite samples measured at 25 °C were obtained and summarised in Table S3. The fractional atom positions (*x, y, z*), site occupation factor (SOF) and isotropic temperature factor or thermal parameters (B_{eq}) of the H-ZSM-5 sample pre-adsorbed with ethanol are given in Table S4. For the H-ZSM-5 sample pre-adsorbed with DMF, the atomic parameters measured at 25 °C are presented in Table S5. For the H-ZSM-5 sample pre-adsorbed with limited ethanol and DMF, the atomic parameters are presented in Table S6.

Table S3. Basic crystallographic data of the H-ZSM-5 samples measured at 25 °C, dehydrated, pre-adsorbed with ethanol, DMF and with a limited mixture of DMF and ethanol.

Samples	H-ZSM-5 (dehydrated)	H-ZSM-5 (ethanol adsorbed)	H-ZSM-5 (DMF adsorbed)	H-ZSM-5 (DMF & ethanol co-adsorbed)
Chemical formula	$H_{4.48}Al_{4.48}Si_{91.52}O_{192}$	$H_{4.48}Al_{4.48}Si_{91.52}O_{192}$ -$n$$C_2H_5OH$	$H_{4.48}Al_{4.48}Si_{91.52}O_{192}$ -$n$$C_6H_8O$	$H_{4.48}Al_{4.48}Si_{91.52}O_{192}$ -$m$$C_6H_8O$.$n$$C_2H_5OH$
Temperature (°C)	25(2)	25(2)	25(2)	25(2)
Wavelength (Å)	0.825634(2) (synchrotron)	0.825850(2) (synchrotron)	0.825850(2) (synchrotron)	0.825850(2) (synchrotron)
2θ -zero point (°)	-0.002500(10)	0.010275(10)	0.010275(10)	0.010275(10)
Space group	*Pnma*	*Pnma*	*Pnma*	*Pnma*
Crystal system	Orthorhombic	Orthorhombic	Orthorhombic	Orthorhombic
a (Å)	20.13675(3)	20.12191(3)	20.16651(4)	20.09515(4)
b (Å)	19.95928(3)	19.93057(3)	19.97710(4)	19.96020(4)
c (Å)	13.43725(2)	13.42604(2)	13.45305(3)	13.43518(3)
V (Å^3)	5400.631(22)	5384.394(15)	5419.812(19)	5388.893(22)
2θ range for refinement (°)	3-55	3-55	3-55	3-55
Detector	Multi-analyser crystals	Multi-analyser crystals	Multi-analyser crystals	Multi-analyser crystals
Number of parameters	36	170	161	153
Number of hkls	4190	4190	4190	4190
Refinement methods	Le Bail	Rietveld	Rietveld	Rietveld
$R_{wp}/R_p/R_{exp}$ (%)	6.621/5.077/4.958	7.649/5.808/3.364	8.457/6.461/3.339	8.955/7.030/3.883
X^2	1.335	2.274	2.533	2.306

Table S4(a). Atomic parameters from the Rietveld refinement of H-ZSM-5 pre-adsorbed with ethanol measured at 25 °C (R_{wp} = 7.649%, R_{exp} = 3.365%, X^2= 2.274).

Species	Atom	*X*	*y*	*z*	SOF	B_{eq} (Å^2)	Wyckoff
Framework	O1	0.37346(45)	0.05149(62)	0.75410(57)	1	2.099(23)	8d
	O2	0.30627(54)	0.05716(52)	0.92008(54)	1	2.099(23)	8d
	O3	0.19923(44)	0.05827(45)	0.02005(40)	1	2.099(23)	8d
	O4	0.09506(38)	0.06229(55)	0.91329(62)	1	2.099(23)	8d
	O5	0.11620(45)	0.04839(55)	0.72565(57)	1	2.099(23)	8d
	O6	0.24673(40)	0.06016(59)	0.75345(55)	1	2.099(23)	8d
	O7	0.37308(47)	0.84215(49)	0.76509(66)	1	2.099(23)	8d
	O8	0.30857(52)	0.84282(39)	0.93245(57)	1	2.099(23)	8d
	O9	0.19539(50)	0.84636(32)	0.03209(49)	1	2.099(23)	8d
	O10	0.08777(43)	0.83897(46)	0.92199(71)	1	2.099(23)	8d
	O11	0.11477(44)	0.83726(45)	0.74053(63)	1	2.099(23)	8d
	O12	0.23986(44)	0.84962(49)	0.75554(69)	1	2.099(23)	8d
	O13	0.31079(46)	0.94840(46)	0.81731(46)	1	2.099(23)	8d
	O14	0.07952(35)	0.95448(51)	0.82108(57)	1	2.099(23)	8d
	O15	0.42233(46)	0.12706(51)	0.60269(64)	1	2.099(23)	8d
	O16	0.40969(50)	1.00129(50)	0.58709(68)	1	2.099(23)	8d
	O17	0.40488(47)	0.86747(49)	0.57131(73)	1	2.099(23)	8d
	O18	0.19211(58)	0.12849(43)	0.61891(54)	1	2.099(23)	8d
	O19	0.20463(54)	0.00367(44)	0.59379(61)	1	2.099(23)	8d
	O20	0.20156(57)	0.87023(46)	0.58355(58)	1	2.099(23)	8d
	O21	0.99693(46)	0.04676(56)	0.79233(58)	1	2.099(23)	8d
	O22	0.99505(48)	0.85142(49)	0.79070(59)	1	2.099(23)	8d
	O23	0.41960(66)	0.75	0.64682(83)	1	2.099(23)	4c
	O24	0.19149(82)	0.75	0.64986(75)	1	2.099(23)	4c
	O25	0.28440(61)	0.75	0.05534(83)	1	2.099(23)	4c
	O26	0.10992(66)	0.75	0.0624(10)	1	2.099(23)	4c
	Si1	0.42491(22)	0.05671(31)	0.66327(31)	1	1.049(11)	8d
	Si2	0.27891(19)	0.06068(24)	1.03346(32)	1	1.049(11)	8d
	Si3	0.30834(30)	0.03098(19)	-0.18939(31)	1	1.049(11)	8d
	Si4	0.11967(22)	0.06401(25)	0.02769(34)	1	1.049(11)	8d
	Si5	0.07071(23)	0.02983(22)	0.81467(35)	1	1.049(11)	8d
	Si6	0.18862(25)	0.05696(25)	0.67589(30)	1	1.049(11)	8d

	Si7	0.42292(24)	0.82909(23)	0.67228(37)	1	1.049(11)	8d
	Si8	0.30910(28)	0.87051(22)	0.81671(30)	1	1.049(11)	8d
	Si9	0.27422(21)	0.82685(21)	0.03309(35)	1	1.049(11)	8d
	Si10	0.12073(24)	0.82612(22)	0.03050(36)	1	1.049(11)	8d
	Si11	0.07261(23)	0.87075(27)	0.82161(35)	1	1.049(11)	8d
	Si12	0.18757(27)	0.82643(19)	0.68213(33)	1	1.049(11)	8d
Ethanol1	O1	-2.10743	0.75557	1.25099	0.3825(68)	20.0(17)	4c
	H2	-2.08704	0.79846	1.28459	0.3825(68)	24.0(20)	4c
	C3	-2.09765	0.76177	1.14514	0.3825(68)	26.0(22)	4c
	H4	-2.07417	0.80486	1.13039	0.3825(68)	30.0(26)	4c
	H5	-2.07024	0.7233	1.12067	0.3825(68)	30.0(26)	4c
	C6	-2.16377	0.76131	1.09357	0.3825(68)	28.0(24)	4c
	H7	-2.16968	0.80418	1.0559	0.3825(68)	34.0(29)	4c
	H8	-2.16578	0.72262	1.04625	0.3825(68)	34.0(29)	4c
	H9	-2.2	0.75683	1.14412	0.3825(68)	34.0(29)	4c
Ethanol2	O1	0.02961	0.32422	1.47871	0.5969(53)	15.12(73)	4c
	H2	-0.00282	0.2861	1.45523	0.5969(53)	18.15(88)	4c
	C3	-0.01034	0.37741	1.51974	0.5969(53)	19.66(95)	4c
	H4	-0.05837	0.36484	1.51561	0.5969(53)	22.7(11)	4c
	H5	0.00216	0.38479	1.59099	0.5969(53)	22.7(11)	4c
	C6	0.00129	0.4407	1.46185	0.5969(53)	21.2(10)	4c
	H7	-0.04156	0.45625	1.432	0.5969(53)	25.7(12)	4c
	H8	0.019	0.47618	1.50733	0.5969(53)	25.7(12)	4c
	H9	0.03419	0.43192	1.40756	0.5969(53)	25.7(12)	4c
Ethanol3	O1	-0.97621	0.17557	0.64367	0.2723(79)	6.5(12)	4c
	H2	-0.94124	0.13727	0.65542	0.2723(79)	7.9(14)	4c
	C3	-0.96682	0.22492	0.72073	0.2723(79)	8.5(16)	4c
	H4	-0.92979	0.2105	0.76555	0.2723(79)	9.8(18)	4c
	H5	-0.95549	0.26912	0.68985	0.2723(79)	9.8(18)	4c
	C6	-1.02957	0.23174	0.78019	0.2723(79)	9.2(17)	4c
	H7	-1.02043	0.22035	0.85143	0.2723(79)	11.1(20)	4c
	H8	-1.04615	0.27894	0.77568	0.2723(79)	11.1(20)	4c
	H9	-1.064	0.20048	0.75318	0.2723(79)	11.1(20)	4c
Ethanol4	O1	-1.08952	0.17105	0.59341	0.4383(63)	20.0(14)	4c
	H2	-1.05627	0.15065	0.64553	0.4383(63)	24.0(17)	4c
	C3	-1.12174	0.22747	0.63985	0.4383(63)	26.0(18)	4c

H4	-1.10456	0.23299	0.70926	0.4383(63)	30.0(21)	4c
H5	-1.11226	0.26906	0.60068	0.4383(63)	30.0(21)	4c
C6	-1.19533	0.21567	0.64292	0.4383(63)	28.0(20)	4c
H7	-1.21086	0.21594	0.71367	0.4383(63)	34.0(24)	4c
H8	-1.21855	0.25196	0.60507	0.4383(63)	34.0(24)	4c
H9	-1.20571	0.17121	0.61208	0.4383(63)	34.0(24)	4c

Table S4(b). Translational and rotational axes for the matrices describing the adsorbate ethanol molecules, together with their corresponding systematic errors.

	X	*y*	*z*
Translational			
Ethanol1	-2.1074(18)	0.7556(86)	1.2510(23)
Ethanol2	0.02961(88)	0.32422(63)	1.4787(15)
Ethanol3	-0.9762(16)	0.1756(18)	0.6437(25)
Ethanol4	-1.0895(13)	0.1711(18)	0.5934(29)
Rotational			
Ethanol1	190.7(75)	244.1(82)	52.4(27)
Ethanol2	108.3(26)	17.8(23)	-34.8(11)
Ethanol3	-75.5(25)	53.2(29)	-125.6(36)
Ethanol4	-26.9(47)	41.6(39)	-68.7(29)

Table S5(a). Atomic parameters from the Rietveld refinement of H-ZSM-5 pre-adsorbed with DMF measured at 25 °C (R_{wp} = 8.457%, R_{exp} = 3.339%, X^2 = 2.533).

Species	Atom	*X*	*y*	*z*	SOF	B_{eq} (Å^2)	Wychoff
Framework	O1	0.37684(48)	0.05499(68)	0.75255(65)	1	1.832(25)	8d
	O2	0.30932(50)	0.05871(54)	0.92543(59)	1	1.832(25)	8d
	O3	0.19809(46)	0.06165(43)	0.02543(45)	1	1.832(25)	8d
	O4	0.09579(38)	0.05807(57)	0.91475(65)	1	1.832(25)	8d
	O5	0.11354(48)	0.04504(55)	0.72940(62)	1	1.832(25)	8d
	O6	0.24622(43)	0.05293(70)	0.75865(61)	1	1.832(25)	8d
	O7	0.37427(51)	0.84195(50)	0.75952(71)	1	1.832(25)	8d
	O8	0.30251(56)	0.84755(42)	0.93166(61)	1	1.832(25)	8d
	O9	0.19652(51)	0.84845(33)	0.03241(52)	1	1.832(25)	8d
	O10	0.08424(47)	0.84053(46)	0.92706(73)	1	1.832(25)	8d
	O11	0.11719(47)	0.83640(46)	0.74246(67)	1	1.832(25)	8d
	O12	0.24036(48)	0.84717(52)	0.76361(74)	1	1.832(25)	8d
	O13	0.31361(43)	0.95152(49)	0.81623(49)	1	1.832(25)	8d
	O14	0.07984(36)	0.95337(55)	0.82822(55)	1	1.832(25)	8d
	O15	0.41967(48)	0.12367(51)	0.60807(72)	1	1.832(25)	8d
	O16	0.40289(52)	1.00242(54)	0.58739(76)	1	1.832(25)	8d
	O17	0.40537(49)	0.87167(51)	0.57239(75)	1	1.832(25)	8d
	O18	0.19076(60)	0.12924(45)	0.61922(60)	1	1.832(25)	8d
	O19	0.20281(60)	0.00204(48)	0.59549(66)	1	1.832(25)	8d
	O20	0.19965(60)	0.87055(49)	0.58780(60)	1	1.832(25)	8d
	O21	0.99733(51)	0.04932(64)	0.79526(60)	1	1.832(25)	8d
	O22	0.99596(52)	0.85111(52)	0.79386(67)	1	1.832(25)	8d
	O23	0.41913(73)	0.75	0.64018(89)	1	1.832(25)	4c
	O24	0.19650(83)	0.75	0.65447(80)	1	1.832(25)	4c
	O25	0.28593(62)	0.75	0.04753(82)	1	1.832(25)	4c
	O26	0.11467(68)	0.75	0.06522(96)	1	1.832(25)	4c
	Si1	0.42464(26)	0.05924(33)	0.66587(36)	1	0.916(13)	8d
	Si2	0.27852(20)	0.06072(27)	1.03645(34)	1	0.916(13)	8d
	Si3	0.31074(31)	0.02973(21)	-0.18602(36)	1	0.916(13)	8d
	Si4	0.12108(23)	0.06360(28)	0.02698(36)	1	0.916(13)	8d
	Si5	0.06991(25)	0.03036(24)	0.81778(36)	1	0.916(13)	8d
	Si6	0.18663(26)	0.05780(27)	0.67567(33)	1	0.916(13)	8d

	Si7	0.42310(27)	0.82944(23)	0.66747(38)	1	0.916(13)	8d
	Si8	0.30950(30)	0.86991(24)	0.81522(33)	1	0.916(13)	8d
	Si9	0.27425(23)	0.82715(22)	0.03047(38)	1	0.916(13)	8d
	Si10	0.12082(26)	0.82569(23)	0.03173(39)	1	0.916(13)	8d
	Si11	0.07270(25)	0.87069(28)	0.82009(37)	1	0.916(13)	8d
	Si12	0.18727(30)	0.82621(20)	0.68486(35)	1	0.916(13)	8d
DMF 1	O1	-2.10446	0.77858	1.26435	0.4296(35)	14.40(82)	4c
	C2	-2.09845	0.75538	1.16989	0.4296(35)	17.28(98)	4c
	C3	-2.03265	0.74961	1.14424	0.4296(35)	20.2(11)	4c
	C4	-1.996	0.77064	1.2284	0.4296(35)	20.2(11)	4c
	C5	-2.042	0.78776	1.29952	0.4296(35)	17.28(98)	4c
	C6	-2.0255	0.81297	1.40135	0.4296(35)	20.2(11)	4c
	C7	-2.15541	0.73846	1.10309	0.4296(35)	20.2(11)	4c
	H8	-2.0077	0.70499	1.11431	0.4296(35)	24.5(14)	4c
	H9	-1.95627	0.74283	1.26628	0.4296(35)	24.5(14)	4c
	H10	-1.97068	0.81559	1.41013	0.4296(35)	24.5(14)	4c
	H11	-2.04643	0.77829	1.45799	0.4296(35)	24.5(14)	4c
	H12	-2.04713	0.86376	1.41162	0.4296(35)	24.5(14)	4c
	H13	-2.13617	0.72067	1.03018	0.4296(35)	24.5(14)	4c
	H14	-2.18654	0.7838	1.09154	0.4296(35)	24.5(14)	4c
	H15	-2.18585	0.69834	1.13791	0.4296(35)	24.5(14)	4c
DMF 2	O1	-1.96795	0.86786	1.45559	0.4868(31)	14.58(59)	4c
	C2	-1.99818	0.92089	1.49958	0.4868(31)	17.50(70)	4c
	C3	-2.04431	0.89929	1.56778	0.4868(31)	20.42(82)	4c
	C4	-2.0422	0.82845	1.56539	0.4868(31)	20.42(82)	4c
	C5	-1.99493	0.81181	1.49592	0.4868(31)	17.50(70)	4c
	C6	-1.97592	0.74174	1.46863	0.4868(31)	20.42(82)	4c
	C7	-1.9834	0.99274	1.47705	0.4868(31)	20.42(82)	4c
	H8	-2.04797	0.91419	1.6463	0.4868(31)	24.8(10)	4c
	H9	-2.03544	0.79459	1.62906	0.4868(31)	24.8(10)	4c
	H10	-2.00582	0.70573	1.51307	0.4868(31)	24.8(10)	4c
	H11	-1.9223	0.73394	1.48444	0.4868(31)	24.8(10)	4c
	H12	-1.98548	0.73347	1.38808	0.4868(31)	24.8(10)	4c
	H13	-2.01535	1.02549	1.5238	0.4868(31)	24.8(10)	4c
	H14	-1.99351	1.00284	1.39711	0.4868(31)	24.8(10)	4c
	H15	-1.93033	1.00331	1.49347	0.4868(31)	24.8(10)	4c

DMF 3	O1	-1.85598	0.77216	1.31054	0.3328(35)	19.1(12)	4c
	C2	-1.86218	0.71832	1.37145	0.3328(35)	23.0(14)	4c
	C3	-1.8017	0.70143	1.41159	0.3328(35)	26.8(17)	4c
	C4	-1.75547	0.74793	1.37275	0.3328(35)	26.8(17)	4c
	C5	-1.79099	0.78993	1.31164	0.3328(35)	23.0(14)	4c
	C6	-1.76204	0.84717	1.25442	0.3328(35)	26.8(17)	4c
	C7	-1.92586	0.68239	1.39203	0.3328(35)	26.8(17)	4c
	H8	-1.78994	0.69483	1.49083	0.3328(35)	32.6(20)	4c
	H9	-1.72077	0.77931	1.41528	0.3328(35)	32.6(20)	4c
	H10	-1.70781	0.85022	1.26911	0.3328(35)	32.6(20)	4c
	H11	-1.78624	0.89464	1.27807	0.3328(35)	32.6(20)	4c
	H12	-1.77056	0.83919	1.17354	0.3328(35)	32.6(20)	4c
	H13	-1.91651	0.64031	1.44442	0.3328(35)	32.6(20)	4c
	H14	-1.94637	0.66235	1.32122	0.3328(35)	32.6(20)	4c
	H15	-1.96205	0.7178	1.42574	0.3328(35)	32.6(20)	4c

Table S5(b). Translational and rotational axes for the matrices describing the adsorbate DMF molecules, together with their corresponding systematic errors.

	X	*y*	*z*
Translational			
DMF1	-2.10446(84)	0.7786(13)	1.2643(15)
DMF2	-1.96795(73)	0.86786(65)	1.4556(11)
DMF3	-1.8560(13)	0.7722(18)	1.3105(19)
Rotational			
DMF1	-200.1(12)	-4.65(78)	2.17(31)
DMF2	58.57(84)	-33.31(66)	-131.53(89)
DMF3	52.04(81)	-11.1(13)	1.92(13)

Table S6(a). Atomic parameters from the Rietveld refinement of H-ZSM-5 pre-adsorbed with limited DMF and ethanol at 25 °C (R_{wp} = 9.005%, R_{exp} = 5.259%, X^2 = 1.712).

Species	Atom	*X*	*y*	*z*	SOF	B_{eq} (Å^2)	Wychoff
Framework	O1	0.36816(50)	0.06015(63)	0.74449(73)	1	1.718(30)	8d
	O2	0.29519(55)	0.06478(49)	0.91155(70)	1	1.718(30)	8d
	O3	0.20000(50)	0.05169(57)	0.02262(55)	1	1.718(30)	8d
	O4	0.09514(48)	0.05082(62)	0.92036(78)	1	1.718(30)	8d
	O5	0.11615(53)	0.04771(65)	0.71605(74)	1	1.718(30)	8d
	O6	0.23764(47)	0.05105(67)	0.74567(68)	1	1.718(30)	8d
	O7	0.36641(50)	0.84642(51)	0.75978(73)	1	1.718(30)	8d
	O8	0.30329(57)	0.84794(43)	0.92707(66)	1	1.718(30)	8d
	O9	0.20262(55)	0.84233(44)	0.03986(60)	1	1.718(30)	8d
	O10	0.09086(50)	0.83272(51)	0.91736(83)	1	1.718(30)	8d
	O11	0.12136(51)	0.84033(50)	0.72749(78)	1	1.718(30)	8d
	O12	0.23326(48)	0.85372(56)	0.74264(79)	1	1.718(30)	8d
	O13	0.30281(53)	0.95322(54)	0.81407(55)	1	1.718(30)	8d
	O14	0.07423(43)	0.95268(59)	0.82301(67)	1	1.718(30)	8d
	O15	0.41283(52)	0.12406(52)	0.59261(83)	1	1.718(30)	8d
	O16	0.41001(57)	1.00514(57)	0.57015(94)	1	1.718(30)	8d
	O17	0.40626(55)	0.87189(57)	0.57146(90)	1	1.718(30)	8d
	O18	0.18609(56)	0.12848(51)	0.61341(67)	1	1.718(30)	8d
	O19	0.19906(64)	-0.00304(50)	0.59427(70)	1	1.718(30)	8d
	O20	0.20508(62)	0.86455(52)	0.57121(77)	1	1.718(30)	8d
	O21	0.99504(53)	0.04374(66)	0.78773(79)	1	1.718(30)	8d
	O22	0.99488(58)	0.85313(59)	0.78702(77)	1	1.718(30)	8d
	O23	0.42169(75)	0.75	0.6357(11)	1	1.718(30)	4c
	O24	0.19631(92)	0.75	0.65161(94)	1	1.718(30)	4c
	O25	0.29415(80)	0.75	0.0652(10)	1	1.718(30)	4c
	O26	0.11518(73)	0.75	0.0661(11)	1	1.718(30)	4c
	Si1	0.42418(26)	0.05246(32)	0.65964(39)	1	0.859(15)	8d
	Si2	0.27955(24)	0.06519(26)	1.02249(39)	1	0.859(15)	8d
	Si3	0.30701(32)	0.02964(23)	-0.19411(40)	1	0.859(15)	8d
	Si4	0.12224(24)	0.05826(32)	0.02829(39)	1	0.859(15)	8d
	Si5	0.06841(27)	0.02989(26)	0.80727(42)	1	0.859(15)	8d
	Si6	0.18370(26)	0.06265(26)	0.66179(36)	1	0.859(15)	8d

	Si7	0.42446(29)	0.82906(26)	0.66408(41)	1	0.859(15)	8d
	Si8	0.30297(33)	0.86993(27)	0.80714(36)	1	0.859(15)	8d
	Si9	0.27728(26)	0.82723(23)	0.03058(38)	1	0.859(15)	8d
	Si10	0.12154(28)	0.82232(25)	0.02161(41)	1	0.859(15)	8d
	Si11	0.07141(28)	0.86702(30)	0.81750(39)	1	0.859(15)	8d
	Si12	0.18798(31)	0.82429(23)	0.67949(37)	1	0.859(15)	8d
Ethanol1	O1	-2.10464	0.75904	1.22838	0.7520(59)	29.32(94)	4c
	H2	-2.07265	0.80007	1.2183	0.7520(59)	35.2(11)	4c
	C3	-2.13891	0.748	1.13569	0.7520(59)	38.1(12)	4c
	H4	-2.12381	0.78179	1.08559	0.7520(59)	44.0(14)	4c
	H5	-2.1288	0.70191	1.11071	0.7520(59)	44.0(14)	4c
	C6	-2.21247	0.75493	1.15161	0.7520(59)	41.1(13)	4c
	H7	-2.23006	0.79178	1.1086	0.7520(59)	49.8(16)	4c
	H8	-2.23504	0.71192	1.1338	0.7520(59)	49.8(16)	4c
	H9	-2.22141	0.76571	1.22306	0.7520(59)	49.8(16)	4c
DMF1	O1	-3.02226	1.85689	0.49902	0.5396(30)	12.91(65)	4c
	C2	-3.0041	1.79275	0.47906	0.5396(30)	15.49(78)	4c
	C3	-2.95026	1.79157	0.41582	0.5396(30)	18.07(91)	4c
	C4	-2.93442	1.85937	0.39574	0.5396(30)	18.07(91)	4c
	C5	-2.97971	1.89716	0.44815	0.5396(30)	15.49(78)	4c
	C6	-2.98177	1.97213	0.44896	0.5396(30)	18.07(91)	4c
	C7	-3.03791	1.73189	0.5201	0.5396(30)	18.07(91)	4c
	H8	-2.92467	1.74696	0.38672	0.5396(30)	21.9(11)	4c
	H9	-2.89405	1.87804	0.3479	0.5396(30)	21.9(11)	4c
	H10	-2.94125	1.99211	0.40091	0.5396(30)	21.9(11)	4c
	H11	-2.97486	1.99051	0.52649	0.5396(30)	21.9(11)	4c
	H12	-3.03074	1.98949	0.4201	0.5396(30)	21.9(11)	4c
	H13	-3.01277	1.68608	0.49154	0.5396(30)	21.9(11)	4c
	H14	-3.09098	1.73168	0.49643	0.5396(30)	21.9(11)	4c
	H15	-3.03511	1.7327	0.60282	0.5396(30)	21.9(11)	4c

Table S6(b). Translational and rotational axes for the matrices describing the adsorbate molecules, together with their corresponding systematic errors.

	X	*y*	*z*
Translational			
Ethanol1	-2.05677(87)	0.76004(41)	1.1929(17)
DMF1	-1.97832(66)	0.69500(30)	1.45665(90)
Rotational			
Ethanol1	106.3(25)	-4.07(51)	47.9(25)
DMF1	60.80(40)	33.04(50)	-45.36(63)

ONIOM Computational Results

In order to investigate the adsorption behavior of EtOH, DMF and Ethylene in the pores of the zeolite, we used the ONIOM method (Our Own N-layered Integrated Molecular Orbital and Molecular Mechanics), first developed by Morokuma et al.[13]. It is a hybrid method that can be applied to large systems using multiple levels of theory. The ONIOM3 (three-layer) method was used for these calculations, applying Molecular Mechanics (UFF) for the Low-Level calculations, a Semi-Empirical (PM6) method for the Intermediate-Model, and quantum mechanical calculations using the hybrid density functional of Truhlar and Zhao (M06-2X/6-311+G(d,p)) for the High-Level system[14-16]. Figure S8 (a) shows the three-layer partitioning scheme chosen for the system, which consists of an 18-atom High Level, 316-atom Intermediate Level and a 152-atom Low Level model. A single Bronsted acid (BA) site was included at the intersection of straight and sinusoidal channels, adjacent to a framework Al site. All the adsorbates were included in the High-Level of theory.

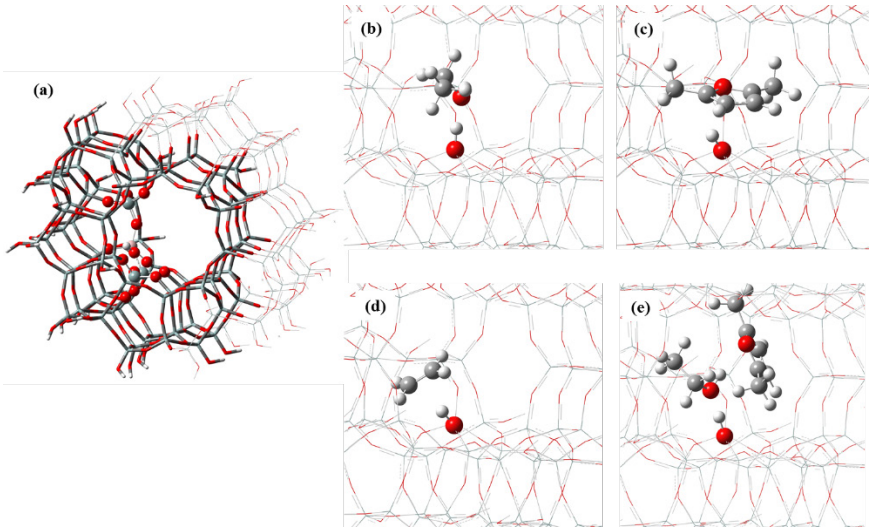

Figure S8: (a) ONIOM3 partitioning scheme applied on the H-ZSM-5 zeolite framework. The different layers are illustrated as follows: High Level with ball-and-stick, Intermediate Level with stick and Low Level with line representations. (b)-(e) Ground state adsorbate conformations of ethanol, DMF, ethylene and ethanol-DMF dimer, respectively. For visual clarity the zeolite framework for all adsorbate configurations is shown in line representation, except for the BA site which is shown in ball and stick (as the adsorbates).

The atoms in the Low and Intermediate layers were kept frozen in their crystallographic positions, while the High-Level atoms were allowed to relax during geometry optimizations. The gas-phase electronic BEs of adsorbates were calculated using the following equation:

$$BE = E_{ONIOM3,ads} - E_{ONIOM3,zeolite} - E_{adsorbate}$$

Where $E_{ONIOM3,ads}$ and $E_{ONIOM3,zeolite}$ are the energies of the adsorbed reactants in the zeolite and the empty zeolite pore system, respectively, and $E_{adsorbate}$ is the (high-level) electronic energy of the adsorbates.

The calculated BEs of individual reactants and the ethanol-DMF dimer within the zeolite pore are shown in Table S7 along with ground state geometries in Figure S8. Our results clearly demonstrate the adsorption preference of EtOH for the BA over ethylene and DMF.

Table S7: Calculated ONIOM BEs of relevant adsorbates in the ethanol and ethylene routes within the H-ZSM-5 pore. Negative values indicate exothermic, while positive values indicate endothermic adsorption.

Species	BE (kJ/mol)
Ethanol	-70.1
DMF	+16.5
Ethylene	-24.1
Ethanol-DMF	-35.8

The calculations demonstrate that ethanol binds the BA site more strongly than ethylene or DMF, with binding energies of -70.1, -24.1 and +16.5 kJ/mol, respectively. (see Table S7 and adsorption geometries in Figure S8). The slightly endothermic value of DMF adsorption compared to the highly exothermic value of EtOH, indicates the steric hindrance of DMF adsorption into the pore of the H-ZSM-5 zeolite. This adsorption preference of EtOH for the BA over the DMF is in perfect agreement with the experimental observations of Fig. 4 in the main manuscript.

In view of the higher adsorption energy of EtOH over Ethylene, there may be a higher local concentration of adsorbed ethanol and dehydrated ‘ethylene’ inside the zeolite cavity from feeding ethanol instead of ethylene gas in their rate comparison (Fig. 2 of main manuscript). This may account for the large difference in their rates despite the fact that the concentration of ethylene (0.45 mol) was actually set higher than ethanol (0.14 mol).

It would be better to carry out detailed kinetic studies over a range of H-USY catalysts with different acid concentrations as that of C.L Williams et al. [10]. But, controlling the quantity of Brønsted acidity in a linear manner while keeping the porous structure intact, in the case of H-USY, may not be easily achieved. Further careful synthesis, characterization and testing of

this catalyst series will be required in future work. On the other hand, we have estimated the acid concentration of our HUSY-12 to be 4.4 mM, which, according to Dauenhauer and coworkers [9,10] is well above the critical concentration hence corresponding to the regime where the cycloaddition is the rate limiting. In addition, the obtained ΔEa = ~44 kJ mol-1 between ethanol and ethylene routes of the same HUSY-12 catalyst from our experiments have also matched well with our theoretical calculations which were based on the assumption of the cycloaddition as the rate limiting. Furthermore, the product selectivities were also consistent with this postulation. Thus, we are confident that the assignment to the cycloaddition as the rate limiting is a corrected assumption.

References:

[1]. C. L. Williams, C.-C. Chang, P. Do, N. Nikbin, S. Caratzoulas, D. G. Vlachos, R. F. Lobo, W. Fan, P. J. Dauenhauer, Catal. Sci. Technol., 2016, 6, 178-187.
[2]. M. F. M. Post, Diffusion in zeolite molecular sieves, in: Introduction to zeolite science and practice, H. van Bekkum, E. M. Flanigen, and J. C. Jansen, eds., vol. 58 of Studies in surface science and catalysis, pp. 391–443, Elsevier, Amsterdam (1991).
[3]. P. A. Jacobs, R.A. van Santen, "Zeolites: Facts, Figures, Future", p 885.
[4]. Y. Zhao, D. G. Truhlar, Theoretical Chemistry Accounts 2008, 120, 215-241
[5]. M. J. Frisch, G. W. Trucks, H. B. Schlegel, G. E. Scuseria, M. A. Robb, J. R. Cheeseman, G. Scalmani, V. Barone, B. Mennucci, G. A. Petersson, H. Nakatsuji, M. Caricato, X. Li, H. P. Hratchian, A. F. Izmaylov, J. Bloino, G. Zheng, J. L. Sonnenberg, M. Hada, M. Ehara, K. Toyota, R. Fukuda, J. Hasegawa, M. Ishida, T. Nakajima, Y. Honda, O. Kitao, H. Nakai, T. Vreven, J. A. J. Montgomery, J. E. Peralta, F. Ogliaro, M. Bearpark, J. J. Heyd, E. Brothers, K. N. Kudin, V. N. Staroverov, T. Keith, R. Kobayashi, J. Normand, K. Raghavachari, A. Rendell, J. C. Burant, S. S. Iyengar, J. Tomasi, M. Cossi, N. Rega, J. M. Millam, M. Klene, J. E. Knox, J. B. Cross, V. Bakken, C. Adamo, J. Jaramillo, R. Gomperts, R. E. Stratmann, O. Yazyev, A. J. Austin, R. Cammi, C. Pomelli, J. W. Ochterski, R. L. Martin, K. Morokuma, V. G. Zakrzewski, G. A. Voth, P. Salvador, J. J. Dannenberg, S. Dapprich, A. D. Daniels, O. Farkas, J. B. Foresman, J. V. Ortiz, J. Cioslowski, D. J. Fox, Gaussian 09 package, 2010.
[6]. C. L. Williams, C.-C. Chang, D. Phuong, N. Nikbin, S. Caratzoulas, D. G. Vlachos, R. F. Lobo, W. Fan, P. J. Dauenhauer, ACS Catal. 2012, 2, 935-939; N. Nikbin, P. T. Do, S. Caratzoulas, R. F. Lobo, P. J. Dauenhauer, D. G. Vlachos, J. Catal. 2013, 297, 35-43.
[7]. H. P. Hratchian, H. B. Schlegel, J. Chem. Phys 2004, 120, 9918-9924.
[8]. J. A. F. Montgomery, M. J.; Ochterski, J. W.; Petersson, G. Alfonso, D., J. Chem. Phys, 1999, 110 (6),2822−2827.
[9]. P. Kostestkyy, J. P. Maheswari, G. Mpourmpakis, J. Phys. Chem. C 2015, 119, 16139-16147.
[10]. S. P. Thompson, J. E. Parker, J. Marchal, J. Potter, A. Birt, F. Yuan, R. D. Fearn, A. R. Lennie, S. R. Street, C. C. Tang, J. Synchrotron Radiat. 2011, 18, 637-648.
[11]. N. H. Heo, C. W. Kim, H. J. Kwon, G. H. Kim, S. H. Kim, S. B. Hong, K. Seff, J. Phys. Chem. C 2009, 113, 19937-19956.
[12]. D. Thompson, D. E. Cox, J. B. Hastings, J. Appl. Crystallogr. 1987, 20, 79-83.

[13] K. Morokuma, R. D. Froese, S. Dapprich, I. Komaromi, D. Khoroshun, S. Byun, D. G. Musaev, C. L. Emerson, Abstracts of Papers of the American Chemical Society 1998, 215, U218-U218.
[14] J. J. P. Stewart, Journal of Molecular Modeling 2007, 13, 1173-1213.
[15] A. K. Rappe, C. J. Casewit, K. S. Colwell, W. A. Goddard, W. M. Skiff, J. Am. Chem. Soc. 1992, 114, 10024-10035.
[16] Y. Zhao, D. G. Truhlar, Theoretical Chemistry Accounts 2008, 120, 215-241.